KSME

Springer

Journal of Mechanical Science and Technology 34 (7) 2020

Original Article
DOI 10.1007/s12206-020-0627-0

Keywords:
· Magneto-rheological fluid damper
· Design parameter optimization
· Design of experiment
· Permanent magnet
· Damping force

Correspondence to:
Jung Woo Sohn
jwsohn@kumoh.ac.kr

Citation:
Olivier, M., Sohn, J. W. (2020). Design and geometric parameter optimization of hybrid magneto-rheological fluid damper. Journal of Mechanical Science and Technology 34 (7) (2020) 2953~2960.
http://doi.org/10.1007/s12206-020-0627-0

Received March 1st, 2020
Revised April 13th, 2020
Accepted April 23rd, 2020

† Recommended by Editor Seungjae Min

Design and geometric parameter optimization of hybrid magneto-rheological fluid damper

Munyaneza Olivier and Jung Woo Sohn

Department of Mechanical Design Engineering, Kumoh National Institute of Technology, Gumi, Gyeongbuk 39177, Korea

Abstract A hybrid type magneto-rheological (MR) fluid damper based on electromagnet and two permanent magnets apart from electromagnet was designed and its characteristics were analyzed numerically. In the proposed MR damper, the magnetic field is generated by the permanent magnet and raised by the additional electromagnet. This combination provides a larger amount of damping force with lower consumption of electric energy. The proposed model has an additional advantage of providing a moderate damping force in case of electromagnet failure. The magnetic circuit of a hybrid MR valve was analyzed by applying Kirchhoff's law and magnetic flux conservation rule. A 2D axisymmetric model of the proposed hybrid MR damper was developed in commercial software where magnetic field properties are analyzed by finite element method. The optimization process was developed to optimize the geometric parameters and generated damping force using design of experiment (DoE) technique. The damping force of the MR damper was selected as an objective function. The optimal solution to the optimization problem of the hybrid MR valve structure was evaluated and compared with the solution obtained from the initial parameters. It is demonstrated that the novel hybrid type provides higher damping force than the previous model.

1. Introduction

MR fluids are smart and controllable materials. The sudden change of MR behavior due to external stimulus makes it more attractive for damping and dissipative devices [1]. It was first developed in 1949 by Jacob Rainbow at the US National Bureau of Standards [2, 3]. The significant advantages of MR fluid attract many engineers and manufacturing industries. MR fluids are used in various areas such as automotive suspension for passengers [4, 5], heavy vehicles [6], military weapons [7], washing machines [8, 9] and human implants such as prosthetic limbs [10]. For the past decades, many works about the design of various types of dampers and different control technics have been carried out. However, most researchers did not pay attention to the hybrid type of MR damper. Lee et al. [11] proposed a novel type of tunable MR damper operated based solely on the location of a permanent magnet incorporated into the piston. Hu et al. [12] proposed a self-sensing MR damper which consists of conventional damper parts and a self-sensing mechanism. Due to the fail-safe problem of existing MR dampers, different designs were proposed to overcome the problem. Xiao et al. [13] proposed a solution for a fail-safe problem by integrating permanent magnets into existing MR damper. Bai and Wereley [14] presented a fail-safe concept that could produce a great dynamic range at all piston speeds. Also, a biased damping force can be generated by permanent magnet which enables fail-safe behavior in case of power loss. In their work, the magnetic field is generated by an electric current through the coil and guided by ferromagnetic poles to the MR fluid gap.

Due to the crucial importance of the magnetic circuit in an MR damper, many researches based on electromagnet have been carried out. However, this model has some drawbacks in terms of energy-saving and fail-safe behavior. For the first problem, the electric current is permanently supplied even on a smooth road at low speed. In the second one, in case of power failure in the coil, the magnetic field is no longer supplied to the MR channel, which causes the damping force to drop to the lowest amount. Till now, very few types of researches concerning hybrid type MR damper have been published. Wulff et al. [15] proposed a vibration damper, in particular for motor vehicles. That work introduced a permanent magnet for supplying a permanent magnetic in case of failure or malfunction of the electric coil. The current research was conducted by Boese and Ehrlich [16] where novel concepts of magnetic circuits were introduced. The basic magnetic field was generated by a permanent magnet and raised by the additional electromagnet. Surprisingly, this novel type of hybrid damper offers better safe-failure and larger damping force. However, in Ref. [16] their model lacks compactness, which limits its wide application.

The main contribution of this work is to propose optimal geometric design parameters and to evaluate the performance of hybrid type MR damper including both permanent magnets and electromagnet. The design objectives of this work were to optimize geometric parameters of MR damper to achieve improved damping force, better dynamic range and provide a fail-safe solution in case of electromagnet failure for vehicle application. The optimization of the hybrid MR damper is based on the design of experiment (DoE) using Box-Behnken method and finite element analysis. The MR damper for vehicle suspension designed by Nguyen and Choi [17] was considered for optimized results comparison.

2. Design and modeling

A schematic diagram of the hybrid MR damper which is operating in valve flow mode is illustrated in Fig. 1. As demonstrated, the hybrid MR damper consists of MR fluid, two permanent magnets, annular gap, electromagnet coil, piston rod, gas chamber, floating piston and casing (cylinder housing). The piston valve is made by two permanent magnets at the bottom and top parts of the electromagnet coil which first generates a permanent magnetic field. The produced permanent magnetic field is strengthened by the electromagnet after adjusting the input current. MR fluid fills the annular gap between the piston and flux return ring. The piston seal between the piston and cylinder housing is used to reduce friction and prevent magnetic leakage. As the piston moves into the damper housing, MR fluid flows through the annular gap. Thus, a pressure drop due to flow resistance of MR fluids in the annular gap is induced [18]. The dimensions for radius and the total height of the MR valve are adopted from Nguyen and Choi [17].

2.1 Magnetic circuit theory

The purpose of this magnetic circuit is to find analytically the relationship between the applied electric current to the coil and the output magnetic flux density and intensity, which play a big role in the change of yield stress of the MR fluid. For this damper, the magnetic field is generated by permanent magnets and boosted by the variation of electric current in the coil. The magnetic field generated is distributed through the annular gap and perpendicular to the MR fluid flow. Fig. 2 shows the cross-sectional diagram of the hybrid MR damper, the corresponding dimensions are shown in Table 1.

Table 1. Geometric dimensions of hybrid MR damper.

Parameters	Symbols	Dimensions
MR fluid gap	g	1 mm
Coil width	W_C	1.5 mm
Height of magnet	H_m	4 mm
Flux return	T_C	5 mm
Piston radius	R	17 mm
Coil radius	R_C	14 mm
Main pole	L_P	6 mm
Small pole	$L_{P'}$	5 mm
Piston shaft radius	R_O	6 mm
Total length	L	50 mm

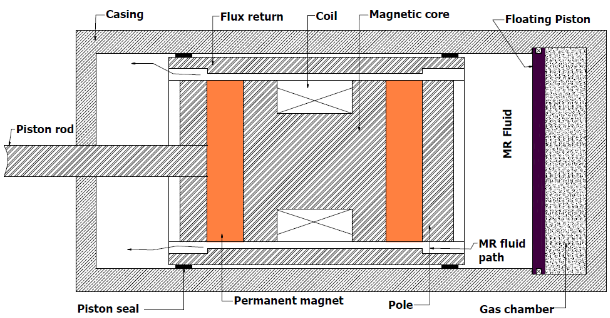

Fig. 1. Schematic diagram of the proposed hybrid MR damper.

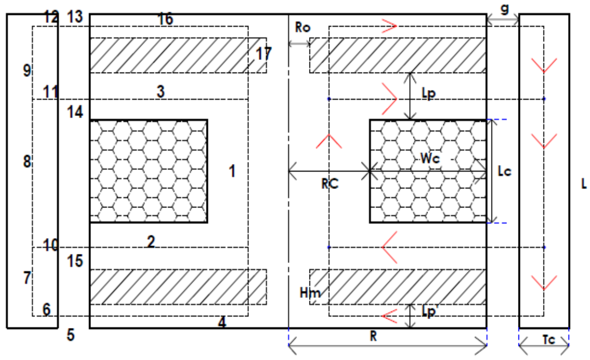

Fig. 2. Cross-section view of hybrid magnetic circuit of piston.

The geometric valve is composed of the piston length (L), MR fluid gap (g), coil radius (R_C), coil width (W_C), magnet height (H_m), flux return thickness (T_C), piston radius (R), piston shaft radius (R_0), length of the main pole (L_P) and length of small pole ($L_{P'}$). Kirchhoff's law and Gauss's law are used analytically to find the magnetic field applied in the annular gap [19]. The magnetic circuit is composed of 17 paths for easy calculation. Fig. 3 of the electric circuit equivalent is

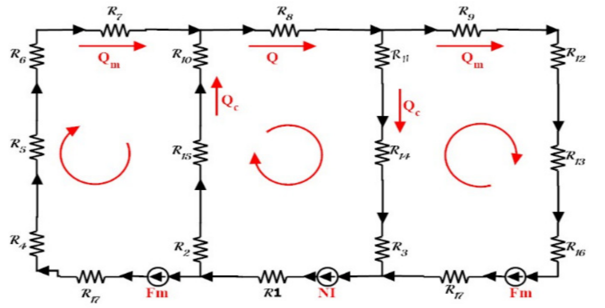

Fig. 3. The equivalent magnetic circuit of piston.

sketched based on those paths. The equivalent magnetic reluctances are calculated as follows:

$$R_1 = \frac{L_C + L_P}{\mu_0 \mu_s \pi R c^2} \tag{1}$$

$$R_{2,3} = \frac{\left({R_C}/{2} + W_C \right)}{\mu_0 \mu_s \pi L_P} \tag{2}$$

$$R_{4,16} = \frac{\left({R_C}/{2} + W_C \right)}{\mu_0 \mu_s \pi R L_{P'}} \tag{3}$$

$$R_{5,13} = \frac{g}{\mu_0 \mu_{MR} \pi \left(R + {g}/{2} \right) L_{P'}} \tag{4}$$

$$R_{6,12} = \frac{{T_C}/{2}}{\mu_0 \mu_s \pi \left(R + g + \frac{3}{4} T_C \right) L_{P'}} \tag{5}$$

$$R_{7,8,9} = \frac{L - L_{P'}}{\mu_0 \mu_s \pi \left[\left(R + g + T_C \right)^2 - \left(R + g + \frac{T_C}{2} \right)^2 \right]} \tag{6}$$

$$R_{10,11} = \frac{{T_C}/{2}}{\mu_0 \mu_s \pi \left(R + g + \frac{3}{4} T_C \right) L_P} \tag{7}$$

$$R_{14,15} = \frac{g}{\mu_0 \mu_{MR} \pi \left(R + {g}/{2} \right) L_P} \tag{8}$$

$$R_{17} = \frac{H_m}{\mu_0 \pi \left(R^2 - R_0^{\ 2} \right)} \tag{9}$$

where μ_0 the magnetic permeability of vacuum which is approximated as $4\pi * 10^{-7}$ H/m . μ_s and μ_{MR} are the relative permeability of low carbon steel and MR fluid, respectively. Low carbon steel has been chosen as the lower the carbon content the better for the electromagnetic core. A neodymium (NdFeB-35) type of magnet was used to generate a significant magnetic field. Also, the type of MR fluid used in this work was MRF-132DG from LORD Co. The magneto-motive force (F_m) was derived from Fig. 3 using Kirchhoff's law as follows:

$$\sum_{i=1}^{m} F_{mi} = \sum_{i=1}^{m} \Phi_i R_{mi} = \sum_{i=1}^{k} N_i I_i \tag{10}$$

From Gauss law, in a given section of the magnetic circuit, F_{mi} is magneto-motive force, N_i is the number of coil turns, $\Phi = \int_A \vec{B}.\vec{d}S$ and I_i is current input. From the electric equivalent shown in Fig. 3, Kirchhoff's voltage law gives:

$$Fm = 2\left(R_{17} + R_4 + R_5 + R_6 + R_7 \right) \Phi_m - 2\left(R_{10} + R_{14} + R_2 \right) \Phi_c \tag{11}$$

$$NI = \left(R_1 + R_2 + R_{14} + R_{10} \right) \Phi_c + R_8 \Phi \tag{12}$$

$$\Phi = \Phi_m + \Phi_c \tag{13}$$

where Φ_C and Φ_m are the magnetic flux values in coil and magnet, respectively. By combining Eqs. (11)-(13), the following equation can be obtained:

$$\Phi_C = \frac{NI - \frac{1}{2} \left(\frac{R_8}{R_{17} + R_4 + R_5 + R_6 + R_7} \right) Fm}{\left(R_1 + R_2 + R_{14} + R_{10} + R_8 \right) + \left(\frac{R_8}{R_{17} + R_4 + R_5 + R_6 + R_7} \left(R_{F_{10}} + R_{E_{14}} + R_2 \right) \right.} \tag{14}$$

$$Fm = \frac{B_r l_m}{u_0} \tag{15}$$

$$R_i = \frac{l_i}{u_0 u_i A_i} \tag{16}$$

where *Br* is remnant flux density. which is a measurement of magnetic induction that, after successful magnetization, remains in the magnet. From Ref. [20], they assumed that the magnetic field is uniform and perpendicular to the MR fluid section and the magnetic field density can be expressed as follows:

$$B_{MR} = \frac{\Phi_C}{A_{MR}} . \tag{17}$$

However, since the magnetic characteristics of solid and MR fluid materials are not linear, it is not easy to obtain the precise magnitude of magnetic field from calculations.

2.2 Finite element analysis

To address the magnetic field distribution and magnetic flux density of the MR-piston valve, a finite element model was built using ANSYS MAXWELL software. A 2D axisymmetric model was developed for parametric study. This model was tested to find the magnetic field density, *B,* generated in the MR fluid gap by varying the current input from 0 to 2 A. The magnetic properties of the materials used are shown in Table 2. B-H curves used for S45C low carbon steel and MRF-132 DG were ex-

Table 2. Geometric dimensions of hybrid MR damper.

SN	Specification	Symbol	Value
1	Relative permeability of low carbon steel (S45C)	μ_s	2000 [17]
2	Permeability of vacuum	μ_o	$4\pi *10^{-7}$
3	Relative permeability of MR fluid (Lord 132-DG)	μ_{MR}	4.5 [22]
4	Relative permeability of (NdFeB) magnet	μ_m	1.09
5	Relative permeability of copper wire	μ_c	0.99

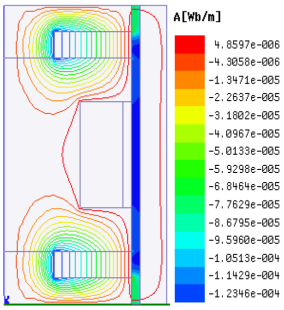

(a) Permanent magnet only

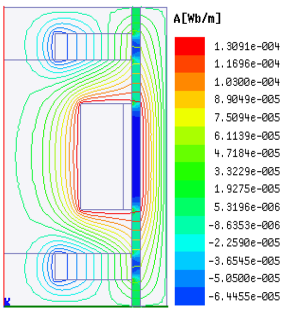

(b) Permanent magnet and electromagnet

Fig. 4. Finite element analysis for hybrid MR damper.

tracted from Refs. [11, 21], respectively. Fig. 4(a) shows the magnetic field lines and magnetic flux density in the MR fluid gap in the case of magnets only. Fig. 4(b) represents both magnets and electromagnets in the working state. The maximum current of 2 A was applied to the coil of 120 turns. To strengthen or weaken the magnetic field of a permanent magnet, the polarity of input excitation counts a great deal. In this study, positive polarity was kept.

To determine the damping force, the relationship between magnetic flux density, B and yield stress, τ_y, for the LORD MRF-132 DG fluid was examined and is shown in Fig. 5. The yield stress for MRF-132 DG can be determined by the following polynomial [21, 23]:

$$\tau_y(KPa) = 52.962B^4 - 176.51B^3 + 158.79B^2 + 13.708B + 0.1442. \tag{18}$$

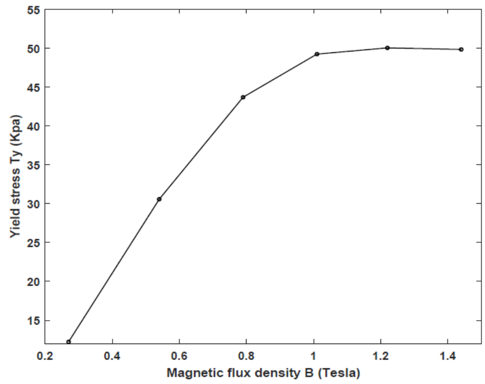

Fig. 5. The relationship between magnetic flux density and yield stress.

The values of yield stress obtained from the above Eq. (18) are used to evaluate the pressure drop of hybrid MR damper as the following equations [23, 24].

$$\Delta P = \Delta P_{vis} + \Delta P_{MR} = \frac{12\eta h}{\pi g^3 R_1} Q + 2C\frac{\tau_y}{g}(L_P + L_{P'}) \tag{19}$$

where ΔP_{vis} and ΔP_{MR} are the viscous pressure drop and field-dependent of MR damper. η is the plastic viscosity of MR fluid, g is the MR annular gap, h is the valve height, and L is flange thickness (pole). R_1 is the average radius of the annular gap and is given by ($R_1 = R + 0.5$ g) Q is the flow rate through the MR valve and can be calculated by $(Q = V_P.A)$. L_P and $L_{P'}$ are the flanges between coil and magnets and flanges at the bottom and top of magnets, respectively. C is a coefficient that depends on the flow velocity profile, its value range between (2.07-3.0), and it can be approximated by the following equation [25]:

$$C = 2.07 + \frac{12Q\eta}{12Q\eta + 0.8\pi R_1 g^2 \tau_y}. \tag{20}$$

The total damping force, *F*, of hybrid MR fluid damper is calculated as follows:

$$F = F_{vis} + F_{MR} = \frac{12\eta H V_P}{\pi g^3 R_1} A^2 + \frac{2C}{g}\tau_y (L_P + L_{P'}) A \tag{21}$$

$$A = A_P - A_S \tag{22}$$

$$A_P = \pi(R + g + T_C)^2 \tag{23}$$

$$A_S = \pi R_0^2 \tag{24}$$

where A_P and A_S is the cross-sectional area of piston and piston shaft, respectively. In this work, the plastic viscosity coefficient of MRF-132 DG was taken as $\eta = 0.112$ Pa·s and the velocity of the piston was chosen as V_P = [0 to 0.08 m/s]. Finally, the damping forces were calculated and presented in Table 3.

Table 3. Calculated damping forces for hybrid MR damper with initial design parameters.

Current (A)	Damping force (N)
0	880.3
0.5	1715.9
1.0	2461.2
1.5	2750.44
2.0	3119..05

Table 4. Input parameters and levels for Box-Behnken design.

Parameters	Parameters names	Levels		
		-1	0	+1
MR gap	A	0.5	1	1.5
Main pole	B	5	7	10
Flux return	C	1.5	5	4.5
Coil radius	D	9	15	15
Small pole	E	2	3	4.5

Table 5. ANOVA response surface for the quadratic model.

Source	Sum of squares	Degree of freedom	Mean square	F-value	P-value Prob. > F	Significance
Model	6.403E+007	20	3.202E+006	33.59	< 0.0001	Significant
A	*1.482E+007*	1	*1.482E+007*	*155.45*	*< 0.0001*	
B	*2.001E+006*	1	*2.001E+006*	*20.99*	*0.0001*	
C	*1.245E+006*	1	*1.245E+006*	*13.06*	*0.0013*	
D	*4.975E+006*	1	*4.975E+006*	*52.19*	*< 0.0001*	
E	*1.718E+006*	1	*1.718E+006*	*18.02*	*0.0003*	
AD	*3.030E+006*	1	*3.030E+006*			
AE	*1.858E+006*	1	*1.858E+006*			
CE	*6.817E+005*	1	*6.817E+005*			
A^2	*3.862E+006*	1	*3.862E+006*			
E^2	*4.869E+005*	1	*4.869E+005*			
Residual	2.383E+006	25	95325.59			
Lack of fit	*2.367E+006*	23	*1.029E+005*	*12.95*	*0.0741*	Not significant
Pure error	*15892.98*	2	*7946.49*			
Cor. Total	6.642E+007	45				

R-square: 0.9641, Adj R-square: 0.9354,
Pre-R-square: 0.7810, Adeq precision 23.532

3. Parameter optimization

The optimization process is developed to optimize the geometric parameters and generated the maximum damping force of hybrid MR damper using response surface method (RSM) and Box-Behnken design. The yield stress force of a hybrid MR damper is selected to be an objective function. In this work, 46 FEM models based on Box-Behnken were developed on ANSYS MAXWELL software to achieve our objective function.

From Table 1, there are ten basic geometric parameters that have a direct effect on the magnetic flux density and the yield stress force. The parameter for permanent magnet, such as height of magnet, is kept constant at a small dimension to avoid high yield stress, which can reduce the riding comfort [17]. Since the weight of damper is increased due to the permanent magnet, the parameters related to the size and weight of the damper, such as coil width, piston radius, piston shaft radius and total length were also kept at a small value. Finally, five design variables were selected at MR gap, g, main pole, L_P, flux return, T_C, coil radius, R_C and small pole $L_{P'}$. During optimization, when there are many factors and interactions which affect the desired response, RSM is an effective tool for optimizing the process [26]. In this optimization, Box-Behnken design was selected as each numeric factor is varied over three levels and this design has fewer runs than 3-level factorials. The five design variables as cited above were chosen for this Box-Behnken design experiment and assigned as A, B, C, D, E and prescribed into three-level as shown in Table 4. Then, 46 runs trials among 243(3^5) were assigned to the DoE software to determine their optimum levels. The trial version software of Design-Expert was used in this work. The influence of design variables to the response parameters which are damping force and magnetic flux density was performed through analysis of variance (ANOVA).

The ANOVA for response surface quadratic model analysis is summarized in Table 5. The F-value of 33.59 for this model implies that the model is significant. There is only a 0.01 % chance that a model F-value larger than the provided one may occur due to noise. In this analysis, the value of “Prob > F-value” less than 0.05 indicates that the model terms are significant. The value of 78.1 % of Pred R-squared is in reasonable agreement with the Adj R-squared of 93.54 %. The results for the signal to noise ratio come out as 23.532, which is an adequate signal for the model. The second-order polynomial equation, which illustrates the relationship of the five factors with the yield stress force (F_{MR}), is given as:

Table 6. Optimum geometric parameters and solutions for hybrid MR damper.

SN	Parameters	Dimensions
1	MR gap (g)	0.7 mm
2	Main pole (L_P)	6 mm
3	Flux return (T_C)	3 mm
4	Coil radius (R_C)	15 mm
5	Small pole ($L_{P'}$)	3 mm
6	Magnetic flux density (B)	1.2 Tesla
7	Yield stress force (F_{MR})	3501.03 N
8	Total length (L)	46 mm

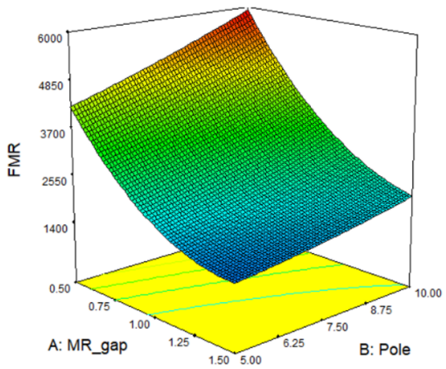

(a) MR fluid gap and main pole to dmaping foce

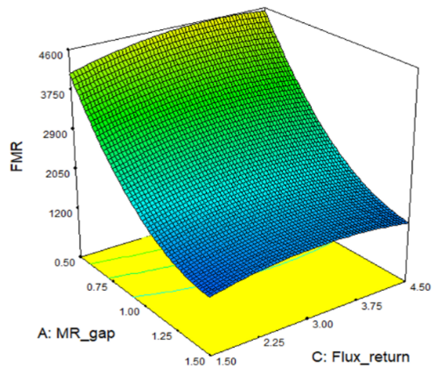

(b) MR fluid gap and flux return to dmaping force

Fig. 6. Interaction effects on damping force.

$$\begin{aligned} \boldsymbol{F}_{MR} = {} & 1924.55 - 1104.97A + 416.39B + 326.4 \\ & +684.99D + 348.32E - 244.97AB - 82.22AC \\ & -752.02AD - 651.14AE + 152.BC + 123.97BD \\ & -66.26BE + 39.32CD + 420.12CE + 90.08DE \\ & +687.57A^2 + 63.84B^2 - 218C^2 + 224.72D^2 \\ & -276.8E^2 . \end{aligned} \tag{25}$$

4. Optimization results

The main purpose of this section is to maximize the damping force while minimizing the damper size. The response surface plots as a function of two factors and maintaining all other factors at fixed values are more useful in getting both the main and the interaction effects of the two factors [27].

Fig. 6(a) shows the interaction effect of MR gap, g, and main pole length, L_P to the damping force, F_{MR}. It is observed that the yield stress is more sensitive to the MR fluid gap with main pole length. Furthermore, the smaller the MR fluid gap and the bigger the main pole length, the higher the generated yield stress force. From Fig. 6(b) a higher yield stress force is generated by gradually decreasing of MR fluid gap while the flux return shows an impact from 2.25 to 3.5 mm thickness and then held constant. In this work, MR gap is the most sensitive parameter to yield stress force. The optimized results of hybrid MR damper parameters with its optimum yield stress force and magnetic flux density are presented in Table 6.

The optimized hybrid MR damper is modeled in ANSYS

Table 7. Total damping force comparison for initial and optimum parameters.

Current (A)	Total damping force from FEM	
	Initial parameters	Optimized parameters
0	880.3 N	1383.2 N
0.5	1715.9 N	2716.2 N
1.0	2461.2 N	3669.7 N
1.5	2750.4 N	4073.3 N
2.0	3119.0 N	4131.4 N

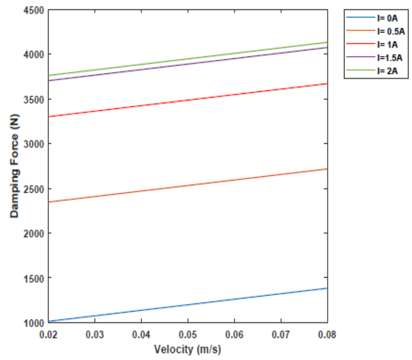

Fig. 7. Damping force against piston velocity at a various applied current.

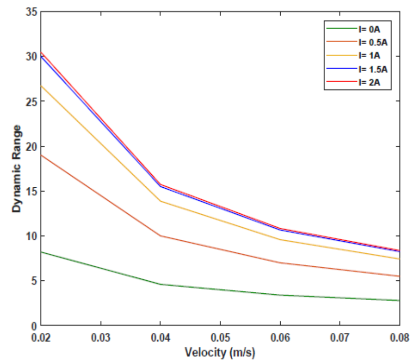

Fig. 8. Dynamic range against piston velocity at a various applied current.

Maxwell platform in a similar way as illustrated for the initial parameters. The total damping force for the optimized damper was calculated by using Eq. (21). The total damping force by FEM was found to be 4131.43 N at a maximum current of 2.0 A. The simulation results for the total damping force versus piston velocity at different applied current are shown in Fig. 7. The increase in external current, the damping force exhibits a gradually increasing trend due to the MR effect. The medium damping force of 1383.21 N at an external current of 0 A shows the impact of permanent magnet in the absence of current and confirm fail-safe stability. From a current of 1.5 and 2.0 A, there are slightly insignificant changes in damping force which indicate that the yield stress approaches its saturation point. To evaluate the performance of hybrid MR damper, the dynamic range, λ_D, which is the ratio of peak force under maximum applied current to that of zero current input. It is calculated as the following [25]:

$$\lambda_D = \frac{F_{viscous+F_{MR}}}{F_{viscous}}. \tag{26}$$

Fig. 8 shows the dynamic range according to velocity at different excitations. At the maximum current of 2.0 A, the dynamic range is 30.35, which implies that the hybrid MR damper exhibits a wide control range. The total damping force for initial and optimized parameter is compared in Table 7. The damping force is clearly much improved after design parameter optimization. For input current of 2.0 A, the damping force is increased 30 % compared to that of initial design.

5. Conclusions

A Hybrid type MR damper was designed, analyzed and numerically simulated. Finite element analysis was used to analyze the model. Box-Behnken design was utilized for optimization. During the optimization process, the effects of pole length, flux return and MR fluid gap on the yield stress force were investigated. The results from the optimized parameters revealed that the damping force varied from 1383 N at the current of 0 A to 4141 N at the current of 2.0 A. The damping force was improved to more than 165 % compared to the previous model with the same size presented by Nguyen and Choi [17].

A moderate damping force of 1383 N at 0 A confirms the excellent fail-safe behavior of our hybrid MR damper. To assure the performance of the damper, a dynamic range of 30.35 at the coil current of 2.0 A and velocity of 0.02 m/s were obtained. The proposed hybrid MR damper will be used for vehicle applications. The next step of this work is to apply this novel type MR damper in a quarter-car suspension for verifying its effectiveness on vibration control.

Acknowledgments

This research was supported by Kumoh National Institute of Technology (2016-104-125).

References

[1] A. Spaggiari, Properties and applications of magnetorheological fluids, *Fracture and Structural Integrity*, 7 (23) (2012) 48-61.
[2] S. E. Premalatha, R. Chokkalingam and M. Mahendran, Magneto mechanical properties of iron-based MR fluids, *American J. of Polymer Science*, 2 (4) (2012) 50-55.
[3] S. K. Mangal and A. Kumar, Experimental and numerical studies of magnetorheological (MR) damper, *Chinese J. of Engineering*, 2014 (2014) 1-7.
[4] G. Z. Yao, F. F. Yap, G. Chen, W. H. Li and S. H. Yeo, MR damper and its application for semi-active control of vehicle suspension system, *Mechatronics*, 12 (7) (2002) 963-973.
[5] J. W. Sohn, J. S. Oh and S. B. Choi, Design and novel type of a magnetorheological damper featuring piston bypass hole, *Smart Materials and Structures*, 24 (3) (2015) 035-013.
[6] H. Sahin, Y. Liu, X. Wang, F. Gordaninejad, C. Evrensel and A. Fuchs, Full-scare magnetorheological fluid dampers for heavy vehicle rollover, *J. of Intelligent Material Systems and Structures*, 18 (12) (2007) 1161-1167.
[7] Z. C. Li and J. Wang, A gun recoil system employing a magnetorheological fluid damper, *Smart Materials and Structures*, 21 (10) (2012) 105003.
[8] A. Ulasyar and I. Lazoglu, Design and analysis of a new magneto rheological damper for washing machine, *Journal of Mechanical Science and Technology*, 32 (4) (2018) 1549-1561.
[9] Q.-H. Nguyen, S. Choi and J. Woo, Optimal design of magnetorheological fluid-based dampers for front-loaded washing machines, *Proceedings of the Institution of Mechanical Engineers, Part C: J. of Mechanical Engineering Science*, 228 (2) (2014) 294-306.
[10] C. Seid, S. Sujatha and S. Sujatha, Optimal design of an MR damper valve for prosthetic knee application, *Journal of Mechanical Science and Technology*, 32 (6) (2018) 2959-2965.
[11] T.-H. Lee, C. Han and S.-B. Choi, Design and damping force characterization of a new magnetorheological damper activated by permanent magnet flux dispersion, *Smart Materials and Structures*, 27 (1) 015013.
[12] G. Hu, Y. Lu, S. Sun and W. Li, Development of a self-sensing magnetorheological damper with magnets in-line coil mechanism, *Sensors and Actuators A; physical,* 255 (2017) 71-78.
[13] P. Xiao, H. Gao and L. Niu, Research on magnetorheological damper suspension with permanent magnet and magnetic valve based on developed FOA-optimal control algorithm, *Journal of Mechanical Science and Technology*, 31 (7) (2017) 3109-3119.
[14] X. Bai and N. M. Wereley, A fail-safe magnetorheological energy absorber for shock and vibration isolation, *J. of Applied Physics*, 115 (17) 17B535.
[15] G. Wulff, A. Thoma, G. Reusing, St. Irmscher and W. Herdeg, Vibration damper, in particular for motor vehicles, *US Patent US5632361A* (1997).
[16] H. Boese and J. Ehrlich, Performance of magnetorheological fluids in a novel damper with excellent fail-safe behavior, *J. of*

Intelligent Material Systems and Structures, 21 (15) (2010) 1537-1542.

[17] Q.-H. Nguyen and S.-B. Choi, Optimal design of MR shock absorber and application to vehicle suspension, *Smart Materials and Structures*, 18 (3) (2009) 035012.

[18] S.-J. Moon, Y.-C. Huh, H.-J. Jung, D.-D. Jang and H.-J. Lee, Sub-optimal design procedure of valve-mode magnetorheological fluid dampers for structural control, *KSCE J. of Civil Engineering*, 15 (5) (2011) 867-873.

[19] T. Avraam, *MR-fluid Brake Design and its Application to a Portable Muscular Rehabilitation Device*, Université Libre de Bruxelles (2009).

[20] J. Zheng, Z. Li, J. Koo and J. Wang, Magnetic circuit sesign and multiphysics analysis of a novel MR damper for applications under high velocity, *Advances in Mechanical Engineering*, 6 (2012) 402501.

[21] S. Purandare, H. Zambare and A. Razban, Analysis of magnetic flux in magneto-rheological damper, *J. of Physics Communications*, 3 (7) (2019) 075012.

[22] W. H. Kim, J. H. Park, S. Kaluvan, Y.-S. Lee and S.-B. Choi, A novel type of tunable magnetorheological dampers operated by permanent magnets, *Sensors and Actuators A; physical*, 255 (2017) 104-117.

[23] Q.-H. Nguyen, Y.-M. Han, S.-B. Choi and N. M. Wereley, Geometry optimization of MR valves constrained in a specific volume using the finite element method, *Smart Materials and Structures*, 16 (6) (2007) 2242-2252.

[24] G. Peng, *Development of MR Fluid Damper for Motorcycle Steering*, University of Wollongong, Australia (2011).

[25] A. Hadadian, *Optimal Design of Magnetorheological Dampers Constrained in a Specific Volume Using Response Surface method*, Concordia University, Canada (2011).

[26] L. Wu, K. Yick, S. Ng and J. Yip, Application of the Box-Behnken design to the optimization of process parameters in foam cup molding, *Expert Systems with Applications*, 39 (9) (2012) 8059-8065.

[27] K. Adinarayana and P. Ellaiah, Response surface optimization of the critical medium components for the production of alkaline protease by a newly isolated Bacillus sp., *J. of Pharmacy and Pharmaceutical Sciences*, 5 (3) (2002) 272-278.

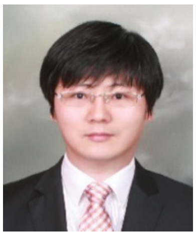

Jung Woo Sohn is an Associate Professor of Mechanical Design Engineering, Kumoh National Institute of Technology, Korea. He received his Ph.D. in Mechanical Engineering from Inha University, Korea. His research interests include smart materials, design and control of smart structures, actuators and sensors for robotics, prognostics, and health management (PHM) and smart system for vehicle applications.